Universiteit Antwerpen

This item is the archived peer-reviewed author-version of:

ZnTi layered double hydroxides as photocatalysts for salicylic acid degradation under visible light irradiation

Reference:
Ciocarlan Radu-George, Wang Hao, Cuypers Bert, Mertens Myrjam, Wu Yan, Van Doorslaer Sabine, Seftel Elena M., Cool Pegie.- ZnTi layered double hydroxides as photocatalysts for salicylic acid degradation under visible light irradiation
Applied clay science - ISSN 0169-1317 - Amsterdam, Elsevier, 197(2020), 105757
Full text (Publisher's DOI): https://doi.org/10.1016/J.CLAY.2020.105757
To cite this reference: https://hdl.handle.net/10067/1735530151162165141

uantwerpen.be
Institutional repository IRUA

ZnTi layered double hydroxides as photocatalysts for salicylic acid degradation under visible light irradiation

Radu G. Ciocarlan[a], Hao Wang[a,b], Bert Cuypers[c], Myrjam Mertens[d], Yan Wu[b], Sabine Van Doorslaer[c], Elena M. Seftel[d,*], Pegie Cool[a]

[a]Laboratory of Adsorption and Catalysis, Department of Chemistry, University of Antwerp, 2610 Antwerp, Belgium

[b]School of Chemistry and Chemical Engineering, Southwest Petroleum University, Chengdu 610500, PR China

[c]Laboratory of Biophysics and Biomedical Physics (BIMEF), Department of Physics, University of Antwerp, 2610 Antwerp, Belgium

[d]VITO Flemish Institute for Technological Research, Boeretang 200, Mol 2400, Belgium

E-mail corresponding author:

Elena M. Seftel: elena.seftel@vito.be

Abstract

A series of ZnTi layered double hydroxides (LDH) with different Zn/Ti ratios are prepared and used as catalysts for photodegradation of salicylic acid (SA) under visible light. The catalysts are characterized by X-Ray diffraction, diffuse reflectance infrared Fourier transform spectroscopy, UV-vis diffuse reflectance spectroscopy, thermogravimetry, electron paramagnetic resonance and N_2 adsorption-desorption. The results show that SA anions bind to the LDH surface and that an electron can be excited from the HOMO in the adsorbed molecules to the conduction band of the LDH under visible light illumination. This charge transfer further leads to an effective photodegradation and mineralization of SA with better conversion results than on P25 titania. Key factors influencing the charge-transfer process in LDH are the high surface area and the Ti/Zn ratio of the LDH materials. The combination of highly dispersed Zn^{2+} and Ti^{4+} cations in the brucite-like sheets of the LDH allows for a better charge separation, which also accounts for the high photocatalytic activity. The present results show that superoxide radicals play a role in the visible-light induced degradation of SA on LDH, while no $^{\bullet}OH$ radicals are formed. In contrast to LDH, the light-induced degradation pathway of SA over P25 titania leads to the formation of CO_2^{-}, a relatively stable anion that may hamper further conversion to CO_2 and hence limit the photocatalytic performance. The introduction of an electron acceptor, such as peroxydisulfate, further improves the degradation and mineralization of SA over LDH, but care should be taken not to use an electron acceptor that can easily adsorb to the LDH surface, such as H_2O_2. ZnTi LDH are thus very promising alternatives to TiO_2 for the photodegradation of colorless organic pollutants, such as SA, under visible light irradiation.

Highlights

- ZnTi layered double hydroxides (LDH) allow mineralization of salicylic acid under visible light
- Visible light induces charge transfer from the adsorbed molecule to the semiconductor
- The Ti/Zn ratio and specific surface area of ZnTi LDH influence the photoactivity
- Photodegradation of SA involves different radical intermediates in LDH than in titania

Keywords layered double hydroxides, visible-light-induced photodegradation, charge transfer, organic pollutant removal

1. Introduction

Photocatalysis has proven to be a very successful tool in environmental remediation to remove organic pollutants in wastewater. In this, TiO_2 is the most widely used photocatalyst due to its activity, non-toxicity, availability, stability and low cost. However, due to its large band gap (E_g=3.2 eV), TiO_2 absorbs less than 5% of the available solar light photons, and is thus only efficient under ultraviolet (UV) light. Therefore, a lot of effort is put in the development of visible-light-sensitive photocatalysts. In general, the strategies to modify TiO_2 for the utilization of visible light for photocatalysis include non-metal and/or metal doping, dye sensitization and coupling of different semiconductors [1]. During the past decades, an alternative form of visible-light activation of TiO_2 has been proposed, namely by exploiting direct charge transfer (CT) between the semiconductor and surface organic adsorbates. Typically, neither the organic adsorbates nor the titania materials are capable of absorbing visible light. But, when placed together, the organic molecules typically adsorb to the semiconductor surface via functional groups such as hydroxyl or carboxyl groups and upon visible light irradiation, an electron is directly photoexcited from the highest occupied molecular orbital (HOMO) of the ligand to the conduction band (CB) of TiO_2 [2]. The thus oxidized adsorbate can be further degraded into smaller molecules and the photo-excited electrons can react with other electron acceptors, such as O_2, to produce oxidizing agents able to degrade different organic molecules. In principle, schemes in which photo-excitation of a valence band (VB) electron in the lowest unoccupied molecular orbital (LUMO) of the absorbent can occur depending on the relative position of HOMO and LUMO versus the CB and VB. This type of CT-mediated photocatalysis has great potential for the degradation of colorless organic pollutants [3, 4]. Note that this mechanism differs from the dye sensitization mechanism, in which the organic molecule (dye) absorbs

visible light. This involves a photoexcited state of the organic molecule which subsequently injects an electron in the CB of TiO_2 [2].

Contamination of urban wastewater by pharmaceuticals and personal care products (PPCPs) poses considerable environmental risks. Among the various PPCPs, salicylic acid (SA) arising from aspirin and cosmetics is found to be one of the pollutants with high occurrence and concentration [5, 6]. As a result, the degradation of SA is of considerable interest. Several authors reported that SA can adsorb on TiO_2 surfaces and lead to CT under visible light illumination [7-11], which can lead to the formation of a visible-light-activated TiO_2 photocatalyst [12, 13] or induce the self-degradation of SA under visible light [4]. However, it is also reported that the coupling between SA and TiO_2 is relatively weak [10], which may limit the photocatalytic activity under visible light [14].

Layered double hydroxides (LDH) are brucite-like lamellar materials constituted by divalent (M^{2+}) and trivalent (M^{3+}) or tetravalent (M^{4+}) metal ions in the sheets which are octahedrally surrounded by oxo bridges and hydroxyl groups, and anions in the interlayer to compensate the excess positive charges of the sheets [15]. Due to the high metal dispersion as MO_6 units within the brucite-like sheets, typical feature of LDH-type structures, the large surface area and better separation from suspension, a wide variety of LDH containing key cations, such as Zn, Ni, Cr, Ti and Sn, have been reported that may be used as effective semiconductor photocatalysts able to degrade organic pollutants in wastewater [16-21].

Most research on CT-driven visible-light-active photocatalysts has been focused on TiO_2, and limited to no attention is paid to LDH. In the current work, ZnTi LDH are used as catalysts for the photodegradation of SA through a CT mechanism under visible light irradiation. The interaction of SA and the LDH surface and the light-induced CT formation is investigated and

compared with those formed on pure TiO_2. To our knowledge, this has not been studied previously.

2. Experimental

2.1. Synthesis of LDH materials

ZnTi LDH with different Zn/Ti ratios ranging from 2 to 4 are prepared by the urea homogeneous co-precipitation method [26, 27]. In a typical synthesis, appropriate amounts of $Zn(NO_3)_2 \cdot 6H_2O$, $TiCl_4$, and urea were dissolved in 100 ml of distilled water and then the solution was stirred vigorously for 1 h. The resulting mixture was transferred into an autoclave and aged at 110 ºC for 24 h. The final products were obtained by filtration, washed several times with water and dried at 80 ºC for 4 h. These samples were denoted as ZnTi-***r***, where ***r*** stands for the final Zn/Ti cationic ratio. All the chemicals were purchased from Sigma-Aldrich and used as received.

P25 (Degussa, Germany) was used as a reference material.

2.2. Characterization techniques

The final ratios of Zn/Ti in the obtained LDH were determined by inductively coupled plasma atomic emission spectrometry (ICP-AES) in an Optima 7300V instrument (Perkin-Elmer, USA).

X-ray diffraction (XRD) was recorded on an X'Pert Pro MPD diffractometer (PANalytical, The Netherlands) with Cu Kα radiation. The measurement was performed in the 2θ mode from 5 to 70º with a scanning speed of 0.04º/4 s.

Diffuse reflectance infrared Fourier transform spectra (DRIFT) were measured on a Nicolet 6700 FTIR spectrometer (Thermo, USA) equipped with a spectra-tech diffuse reflectance accessory. About 200 scans were taken with a 4 cm^{-1} resolution.

Thermogravimetric analysis (TGA) and differential scanning calorimetry (DSC) were performed on a STA-449C (Netzsch, Germany) thermal analyzer at a heating rate of 5 ◦ C/min under air flow.

UV-visible diffuse reflectance spectra (UV-vis DR) were obtained at room temperature on a Thermo-electron evolution 500 UV-vis spectrometer (Thermo, USA), with a diffuse reflectance accessory using KBr as reflectance.

Porosity and surface area were measured on a Quadrasorb SI analyzer (Quantachrome, USA) using N_2 as adsorbate at -196 ^{o}C. Before the measurement, all the samples were outgassed at ambient temperature for 16 h.

X-band light-induced (LI) EPR (electron paramagnetic resonance) experiments were performed at low temperature (10 K) on a Bruker ESP300E spectrometer with a microwave frequency of ~9.45 GHz, equipped with a gas-flow cryogenic system (Oxford Instruments), allowing for operation from room temperature down to 2.5 K. The magnetic field was measured with a Bruker ER035M NMR Gauss meter. The samples were recorded before and after irradiation with 447-nm diode laser light (Dragon Lasers M series) with an output power of 300 mW. Control measurements were performed using the 457.9 nm laser line of a Spectra Physics BeamLok 2060 Ar^+ laser with a power of 10 mW. The EPR spectra were measured with a modulation amplitude of 0.2 mT, a modulation frequency of 100 kHz and a microwave power of 0.5 mW. Care was taken that the same amount of material was used in all experiments. The spectra are simulated using EasySpin [28], a MATLAB (Mathworks, Natick, Massachusetts, USA) toolbox.

2.3. Photodegradation experiments

The photocatalytic activity of the obtained LDH was tested for the photodegradation of SA under visible-light irradiation. A 250W Xenon lamp (Unnasol, Germany) equipped with a cutoff filter

to remove the light below 400 nm was used as light source. The reaction was performed in a 200 ml glass beaker with a water cycling jacket to keep the constant ambient temperature. The amount of 50 mg of catalyst was added to 50 mL SA solution (50 mg/L or 1.0 g/L; unless otherwise mentioned). Unless otherwise indicated, the pH of the initial SA solution was adjusted to 5.2 by NaOH (1 M) to avoid the dissolution of LDH. Prior to visible-light irradiation, the suspension was stirred under dark for 0.5 h to establish the adsorption–desorption equilibrium between SA and the surface of the catalyst. Afterwards, the suspension was irradiated with visible light for 6 h. During the reaction, at intervals of 1 h, ca. 2 mL of the suspension were collected, centrifuged and analyzed at 296 nm with a Thermo-electron evolution 500 UV-vis spectrometer (Thermo, USA). Immediately after the analysis, the sample including solid and liquid was placed back to the reaction system. The total organic carbon content (TOC) of the liquid was measured on a TOC-VCPH analyzer (Shimadzu, Japan). A commercial photocatalyst P25 (Degussa, Germany) composed of 75% anatase and 25% rutile was used as reference. After reaction, the catalysts were collected by filtration, washed with water for several times to remove free SA and then dried at 80 ^{o}C for 4 h.

3. Results

Table 1. Composition, specific surface area and pore volume of the ZnTi LDH under study

	ZnTi-2	ZnTi-3	ZnTi-4	P25
Zn/Ti ratio	2.07	2.90	4.56	-
Ti/Zn ratio	0.48	0.34	0.22	-
Specific surface area (m^2/g)	102	79	59	60

Pore volume (cm^3/g)	0.25	0.22	0.17	0.45

The full XRD and DRIFT analysis of the basic ZnTi LDH materials used in this study are reported in the supplementary material (Section S1). It agrees with earlier reports [26, 27, 29]. In short, the DRIFT experiments show that the electrostatic attraction between the brucite layers and the interlayer carbonate anions is stronger than compared with M^{3+}-containing LDH, which results in a decrease of the symmetry of the carbonated anions from a D_{3h} for the free anions to C_{2v} due to the disordered nature of the interlayer space [18, 27, 29]. These results correlate with the XRD observations indicating a decrease in the interlayer distance due to the higher positive charged brucite-like sheets.

Table 1 lists the final Zn/Ti ratio of the synthesized LDH and reports their porosity characteristics. Note that ZnTi-2 and ZnTi-3 exhibit a higher surface area than the commercial photocatalyst P25 (75% anatase, 25% rutile) that is used in the current study as a reference material.

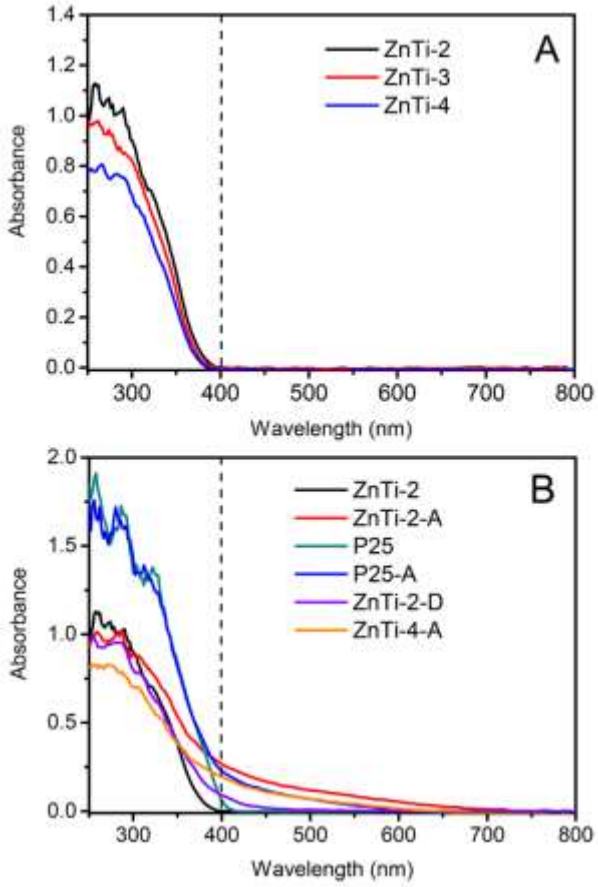

Figure 1. (A) UV-vis DR spectra of the ZnTi LDH before adsorption of SA. (B) Effect of contacting the LDH and P25 for 6h with SA (samples after 6h contact in visible light: ZnTi-*r*-A (*r*=2,4) and P25-A; sample after 6h contact in dark: ZnTi-2-D).

Figure 1A shows the UV-DR spectra of the ZnTi LDH samples under study. All the samples show an intense absorption band at the wavelength below 380 nm, due to the Ti^{4+} and Zn^{2+} in MO_6 octahedral units [31]. Note that the as-prepared ZnTi-LDH photocatalysts exhibit no significant absorption in the visible-light range, which is in agreement with the reported literature data [18, 31]. The decrease in the UV absorption intensity when going from ZnTi-2 to ZnTi-4 may be explained by the increase of the Zn/Ti ratio, *i.e*. the relative decrease in the Ti^{4+} content.

We subsequently tested the photocatalytic activity of the synthesized ZnTi LDH materials towards degradation of SA under visible light illumination (Figure 2). The most commonly used commercial P25 TiO_2 was taken as a reference photocatalyst. In an additional control experiment (not shown), the stability of a solution of SA in visible light was tested. Its concentration remained almost constant when irradiated for 6 h. As shown in Figure 2A, all the as-prepared LDH photocatalysts proved to be very active for photodegradation of SA under visible light illumination and their activity increases with decreasing Zn/Ti ratios. In contrast, commercial P25 showed much poorer photocatalytic activity. Only 10% of SA could be removed from the solution using P25 and the removal degree remained nearly constant after 2 h. In contrast, the most active LDH (ZnTi-2) could remove 40% of SA under the same experimental conditions. Furthermore, the TOC value of the initial SA solution as well as the solution after reaction over P25 and ZnTi-2 was measured. It was found that the TOC removal by ZnTi-2 and P25 after irradiation with visible light for 6 h is 30% and 1%, respectively. This suggests that most SA removed by ZnTi-2 is degraded completely, whereas the use of P25 gives only marginal full degradation of SA.

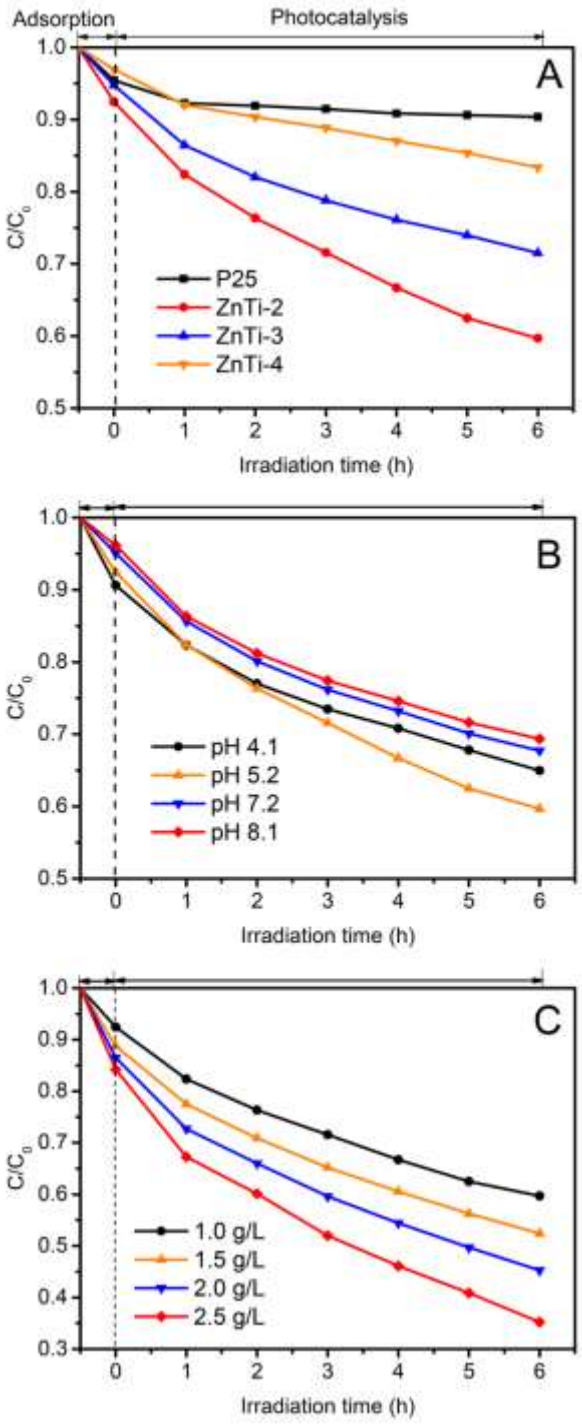

Figure 2. (A) Comparison of the photodegradation of SA over ZnTi LDH and P25 during visible light irradiation. (B) Effect of pH of the initial solution on the photodegradation of SA over ZnTi-2. (C) Effect of the catalyst concentration on the photodegradation (shown for ZnTi-2). SA is first allowed to adsorb to the catalyst in dark during ½ hour prior to light irradiation (marked as adsorption and photocatalysis phase, respectively, in the figures).

All samples were left in contact with the SA solution for ½ hour in dark prior to the photocatalysis experiments. The initial adsorption of pollutants on the catalyst's surface will of course play an important role in the photodegradation reaction. Figure 2A indicates that the amount of initial SA adsorption on the surface of the ZnTi LDH catalysts follows the specific surface area given in Table 1. As a control test, the adsorption of SA was also monitored for 6h in dark to verify that the observed removal of SA under visible light as reported in Figure 2A is not simply due to an on-going adsorption process onto the catalyst's surface (not shown). It was observed that the concentration of SA in solution was nearly the same as the one after adsorption for 0.5 h, indicating that the adsorption equilibrium is reached within 0.5 h. This agrees with similar experiments.

In a second set of experiments, the effect of pH on the photodegradation of SA over ZnTi-2 was tested (Figure 2B). The pH value of the SA solution (50 mg/L) is around 4. Higher pH was adjusted by NaOH (1 M). Figure 2B indicates that the SA removal initially increases with increasing pH, reaches a maximum at pH of 5.2 and then decreases with a further increased pH. The effect of the ZnTi-2 dose on the photo-induced removal of SA was then studied in the range of 1.0-2.5 g/L catalyst at pH 5.2 (Figure 2C). Both the photodegradation activity and the adsorption amount increase when increasing the catalyst dose. At the catalyst dose of 2.5 g/L, 65% SA is removed.

Crucial in understanding the obtained photoactivity is the observation that all the samples changed color, from white to pale orange-red, when contacted with SA. This seems to point to a charge-transfer (CT) process between SA and the LDH surface. As already mentioned in the introduction, such light-induced CT has been observed between SA molecules and a TiO_2 surface

and led to the subsequent photodegradation of the SA molecules [4,10, 13], but it has never been reported for ZnTi LDH.

In order to verify the possible CT mechanism between SA and the LDH under study and to understand the superior photoactivity observed for ZnTi-2, the interaction of both the LDH materials and the P25 reference sample with SA was further characterized. For this, a set of additional materials was prepared. The catalyst (P25, ZnTi-4 or ZnTi-2) was added to an SA solution at pH 5.2 and first stirred under dark for ½ h to reach the adsorption-desorption equilibrium between SA and the catalyst surface, as done in the photocatalysis experiments presented in Figure 2. Afterwards, this suspension was either kept in dark, or illuminated for 5 minutes or 6h with visible light. In the following, the samples will be indicated with the suffix –A (=6h illumination), -D (=6h dark) and –DA (= 5 min visible-light exposure). These samples were then analyzed by UV-vis DR spectroscopy, DRIFT and EPR.

Figure 1B has shown that, in line with the visually observed coloration, the UV-vis DR spectra of ZnTi-2-A, ZnTi-4-A and P25-A extend further in the visible range than those of the pristine materials. This red shift also occurs when ZnTi-2 is contacted with SA for 6h in dark, but to a lower extend which indicates the adsorption of SA on the surface and consequently, the visible-light-induced CT. This effect is further enhanced after exposing the materials to visible light irradiation, as indicated by the UV-vis DR spectra of the ZnTi-2-A sample, confirming their activation in photocatalytic reaction due to the light-induced CT mechanism.

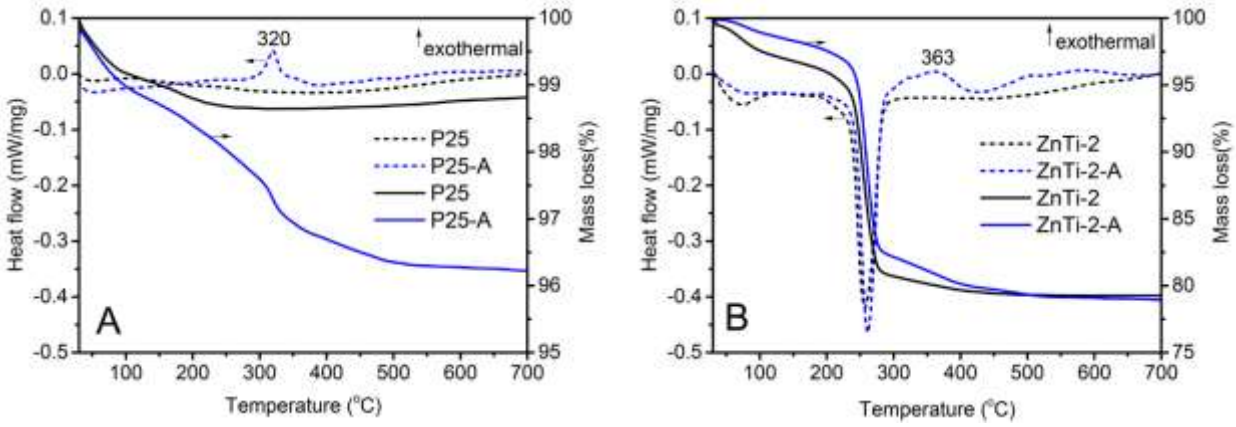

Figure 3. The TGA/DSC profiles of (A) P25 and P25-A and (B) ZnTi-2 and ZnTi-2-A.

Figure 3 shows the TGA/DSC profiles of P25 (A) and ZnTi-2 (B) before and after contacting with SA under visible light. The mass loss observed for P25-A is higher than that of the initial P25 (Figure 3A). For P25-A, an obvious exothermal peak centered at 320 ºC is observed in the DSC curve. This can be caused by the decomposition and consequent combustion of the SA chemically bonded with titanium sites, since free SA decomposes completely below 205 ºC. The TGA/DSC profiles of the pristine ZnTi LDH show two endothermal peaks (Figure 3B, Figure S3): the first one below 200 ºC can be attributed to the release of physically adsorbed as well as interlayer water molecules and the second one, centered about 255 ºC, is attributed to the decomposition of carbonate and dehyroxylation of the brucite-like layers [20]. In contrast, ZnTi-2-A shows additional mass losses above 280 ºC when compared with ZnTi-2 (Figure 3B). Two additional exothermal peaks may be observed for ZnTi-2-A, the first one is centered at 363 ºC and the second one is a broad shoulder in the range of 420-650 ºC. These can be attributed to the decomposition and combustion of SA bonded to the LDH surface. The existence of two extra exothermal peaks may be due to the interaction of the SA with different sites with energetic heterogeneity [7]. The TGA/DSC experiments thus confirm the interaction of SA with the

surface of both ZnTi-2 and P25. Notably, the decomposition and combustion of SA from the ZnTi-2-A sample occurs at much higher temperature than in the P25-A case, indicating that more energy is required to decompose the surface complexes in the former case. It was already observed that ZnAl LDH intercalated with SA by ion exchange or co-precipitation show a higher decomposition temperature for SA than pure SA [31]. Similar effects were observed for SA intercalated in MgAl LDH [31]. However, the XRD pattern of ZnTi-2-A (not shown) matches perfectly with the pristine ZnTi-2 sample, indicating that the SA molecules are not replacing the intercalating carbonate anions in the interlayer gallery. Any interaction of SA with the LDH materials is thus on the surface of the semiconductors.

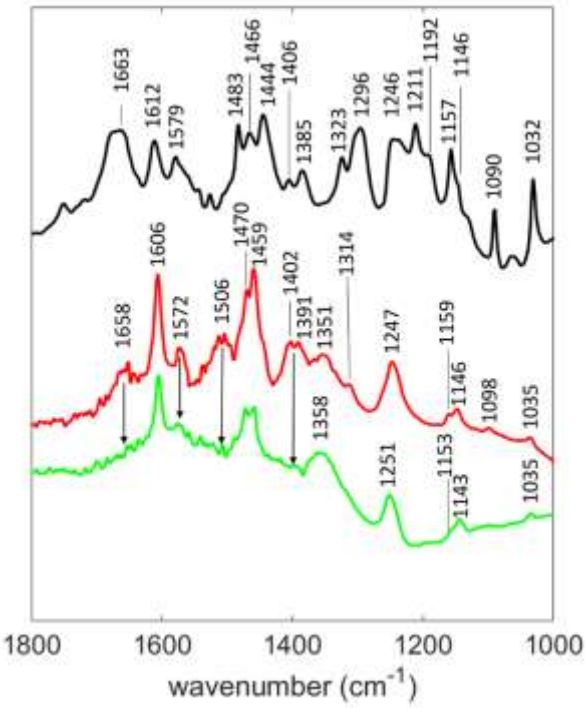

Figure 4. (black, top) DRIFT spectrum of salicylic acid, (middle, red) spectrum obtained by subtracting the DRIFT spectrum of P25 from that of P25-DA and (bottom, green) spectrum obtained by subtracting the DRIFT spectrum of ZnTi-2 from that of ZnTi-2-DA (see supplementary information for details on subtraction).

Fourier-Transform IR spectroscopy is often used to identify the interaction of organic molecules with titania and LDH surfaces [7-9, 13, 14, 31-35]. The most relevant vibrational modes of SA are found in the 1000-1800 cm^{-1} area (Figure 4, top). However, this is exactly the area where the DRIFT spectrum of ZnTi LDH is dominated by the bands of the carbonate anions in the interlayer of the LDH structure (supplementary material (Figures S2, S4), [27, 30]). Figure 4 (bottom) shows the subtraction of the ZnTi-2 DRIFT contribution from the one of ZnTi-2-DA to reveal the additional SA-related spectral contributions. Similar spectra were found for ZnTi-2-A and ZnTi-2-D (supplementary material, Figure S5). The same procedure was used for the P25 case (Figure 4, middle). The DRIFT spectrum of pristine P25 (not shown) has only a weak peak from the bending modes of adsorbed water in the 1625-1640 cm^{-1} region, making spectral subtraction less problematic. The difference spectrum of P25-DA shown in Figure 4 (middle) equals that of P25-D, but changes remarkably for P25-A (supplementary material, Figure S6). This can be due to the build-up of partial degradation products on the titania surface during photocatalysis. Indeed, the earlier discussed photocatalytic experiments revealed that P25 removes 10% SA molecules from the solution, but converts only 1% to CO_2 under visible light, while ZnTi-2 is fully degrading quasi all SA that it removes under the same illumination conditions.

Inspection of Figure 4 immediately reveals that the stretching vibration of the carbonyl group ν(C=O) at ~1663 cm^{-1} reduces considerably after contacting of SA with P25 and ZnTi-2. This is indicative of the deprotonation of the COOH group as a consequence of its binding to Ti ions [7,8]. Similarly, the disappearance of the stretching and bending vibrations of the phenolic OH group (1192, 1211, 1323 and 1385 cm^{-1}) indicates that the phenolic stretching interacts strongly with the semiconductor surface [7,8]. Moreover, the stretching vibrations of the benzene ring,

especially those at 1444 cm^{-1} and 1483 cm^{-1}, are in both the titania and LDH case affected by the interaction of SA with the inorganic surface. The in-plane CH bending modes (at 1032, 1090, 1146 and 1157 cm^{-1}) are less affected. The DRIFT spectrum of P25-DA shown here is in accordance to those of other titania surface-modified with salicylate [7, 8, 35]. Although all these studies agree that the interaction of SA with the titania surface occurs via both the carboxylic and the phenolic group, they differ on the proposed binding models [7-9, 11]. Figure 5 depicts three plausible models. Although some reports point to binuclear bidendate binding (Figure 5, model 3) as the unique interaction mode for TiO_2-SA systems [7, 8], a more complex interaction model implying heterogeneous interaction and various binding sites is more likely [11].

Compared to the DRIFT difference spectrum of P25-DA, the peaks at 1572, 1506, and 1391-1402 cm^{-1} (assigned to the carboxylate symmetric and asymmetric stretching vibrations) seem to disappear in the spectrum of ZnTi-2-DA (Figure 4, arrows). However, these modes fall in the region where the carbonate contributions of the interlayer are situated (Figure S4), and the absence of these peaks may thus be an artifact from the background subtraction. In fact, in the difference spectra of ZnTi-2-D and ZnTi-2-A (Figure S5), weak signals seem still to be present at these positions and we need to be careful in interpreting apparent lack of the peaks. The only clear conclusion based on the here presented DRIFT results is that, similar as for the titania case, binding of SA to the ZnTi LDH surface involves both the phenolic and the carboxylic group. Besides models 1 and 2 shown in Figure 5 and equivalent binding modes to Zn(II), also a bidendate binuclear binding model involving a Ti(IV) and Zn(II) center is possible. The mean distance between two neighboring metal cations, *e.g.* between Zn and Ti cations, in the sheets of ZnTi-2 is 0.308 nm as calculated by the d spacing of (110) crystal plane. Two Ti cations cannot occupy adjacent sites in the sheets due to the electrostatic repulsion [36, 37], hence the distance

between two closest Ti cations will be too large to be bridged by the two O atoms in the phenolic hydroxyl and carboxyl (C-O) of the SA molecule. Interestingly, the FTIR spectra reported for zinc-layered hydroxide-salicylate nanohybrids [33] are also similar to those found here for ZnTi-2 contacted with SA, indicating that the Zn(II) ions are potential binding partners for SA.

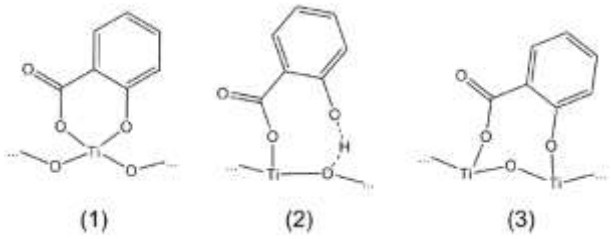

Figure 5. Three proposed binding schemes of salicylate to a TiO_2 surface.

EPR has been shown to be an excellent tool to investigate the formation of light-induced paramagnetic centers, such as organic radicals or Ti^{3+} centers formed during photocatalytic processes in titania materials [38]. This light-induced (LI) EPR technique is here used to further evaluate the effect of light illumination on the ZnTi-2 with and without SA. The experiments are performed at low temperature to slow down the radical reaction kinetics.

In a first step, control experiments are performed on the pristine materials SA and ZnTi-2. No light-induced EPR signals due to radical formation can be observed when SA is irradiated with 447-nm laser light for 0.5 h at 10K (Supplementary material, Figure S7). This confirms the stability of SA against degradation with visible light as also observed in the photodegradation experiments (*vide supra*). Illumination of pristine ZnTi-2 under the same conditions leads to a detectable albeit weak EPR spectrum with three contributions (centers I-III in Table 2, spectrum shown in supplementary material, Figure S8). Center III has the typical *g* values of a Ti(III) center [39, 40]. Ti(III) is formed by trapping of photoexcited electrons by Ti(IV) in the ZnTi-2. The observed *g* values are very close to those found for Ti(III) on bulk lattice trapping sites in

brookite in line with the presence of the TiO_6 octahedra in the LDH [40]. Center I has the characteristic *g* values of $HO_2^{\bullet}$, formed by electron transfer from Ti(III) or conduction band electrons to surface O_2 forming O_2^- that interacts further with surface hydroxyls [41]. These centers are reactive and may initiate the degradation of organic products. A small contribution of an organic radical is found with unknown origin, which may stem from an impurity organic material present in the synthesis glassware. Although the UV-DR spectra show no clear absorption of visible light for pristine ZnTi-2 (Figure 1A), the EPR experiment illustrates that some absorption of 447-nm light with related formation of paramagnetic states occurs. A similar observation has been also made for P25 [42] and was also confirmed in our test measurements of pristine P25 (not shown). This absorption of visible light may be related to defect sites in the material. The effect is, however, negligible in comparison to the response in the UV.

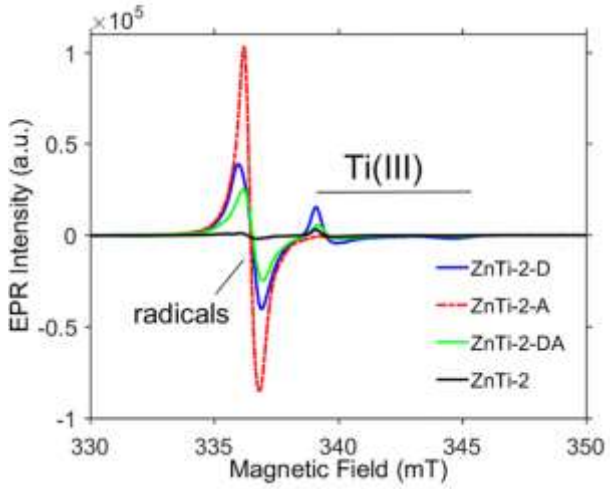

Figure 6. EPR spectra of ZnTi-2 (black, solid), ZnTi-2-A (red, dot-dashed), ZnTi-2-DA (green, solid) and ZnTi-2-D (blue, solid) recorded at 10K after 0.5 h illumination with 447-nm laser light. All spectra were corrected for differences in the microwave frequency to allow facile comparison.

When ZnTi-2 is contacted with SA and then *in-situ* illuminated for 0.5 h at 10K, the LI-EPR response not only increases strongly in intensity, the EPR pattern changes also drastically compared to the pristine ZnTi-2 case (Figure 6 and supplementary material). There is also a

difference whether ZnTi-2 has been mixed with SA in dark (ZnTi-2-D) or in light (ZnTi-2-A and ZnTi-2-DA). When the preparation of the ZnTi-2 sample was performed in dark (ZnTi-2-D), the EPR spectrum consists of a contribution of Ti(III) and two radical-type signals (Table 2, Figure S9). The EPR parameters of the Ti(III) center are close to those observed in the pristine material (Table 2, III'). The dominant contributions to the EPR spectrum stem from organic radicals that are formed due to the degradation of SA. The EPR spectrum of radical center IV has a Lorentzian line shape, suggesting close contact of organic radicals (exchange narrowing through clustering), while this is not the case for center V, which is a more isolated carbon-centered organic radical. When the sample is longer irradiated, the contribution of center V disappears and only signal IV is left (Figure S10). Longer irradiation will generate more organic radicals on the surface that can be in close vicinity at the surface leading to exchange narrowing of the EPR signal.

When the sample has been exposed to sunlight during the preparation, only contributions due to Ti(III) and radical clusters IV are found (Figure 6, Table 2, Figures S11 and S12). The EPR signal of ZnTi-2-A measured before illumination in the EPR cavity shows already a radical contribution (dark signal about 15x higher than observed for ZnTi-2-DA), indicating the formation of SA-related radicals already during the 6h mixing time in light. Subsequent *in-situ* illumination at 10K results in a larger formation of radicals in ZnTi-2-A than in ZnTi-2-DA and ZnTi-2-D, but reveals that the production of the Ti(III) centers is lowest for this sample. This seems to point to an increased transfer of electrons from Ti(III) surface centers to the organic molecules (possibly via a Ti(IV)-O_2^- intermediate), leading to EPR-silent Ti(IV) and radical centers.

A similar illumination at 10K of P25-DA also leads to a huge increase and change of the EPR signal (Figure S13, Table 2). Two signals due to Ti(III) appear upon illumination with the 447-nm laser light (signals VIII and IX). These signals are often detected in P25 during photocatalysis and can be ascribed to Ti(III) in the anatase (VIII) and rutile (IX) phase of the material [40]. Note that the parameters of the Ti(III) centers in the illuminated ZnTi-2 (III and III') differ from those observed in P25, reflecting the different symmetry of the local environment of the Ti atoms in these materials. Furthermore, several EPR signatures due to organic radicals are observed in illuminated P25-DA. Besides $HO_2^{\bullet}$ (center I), there are two contributions that can be assigned to radicals that are reaction products of SA (centers VI and VII). The principal *g* values of center VI are similar to those reported for CO_2^- radicals on different oxides [43]. The EPR parameters of center VII, especially the *g* value around 2.011, could point to formation of $RCO_3^{\bullet}$ radicals [44]. It is important to note that these radicals VI and VII were not observed in the ZnTi-2 cases, indicating a very different photodegrading reaction mechanism.

Table 2. Principal *g* values of the paramagnetic centers contributing to the LI-EPR spectra of ZnTi-2 with and without SA (see supplementary material for simulations). Number in brackets indicates the experimental error on the last digit.

Center	g_1	g_2	g_3	Assignment	Relative spectral contribution (%)
			ZnTi-2		
I	2.0028(5)	2.008(1)	2.034(2)	$HO_2^{\bullet}$	45(1)
II	2.0021(5)	2.0056(5)	2.0068(5)	Organic radical	2(1)
III	1.9885(5)	1.9875(5)	1.9565(5)	Ti(III) (brookite-like)	53(1)

ZnTi-2-D					
IV	2.004 (1)	2.004 (1)	2.004(1)	Radical cluster	72(1)
V	2.0080(5)	2.0070(5)	2.0050(5)	Radical	5(1)
III’	1.9880(5)	1.9860(5)	1.956(1)	Ti(III) (brookite-like)	23(1)
ZnTi-2-DA					
IV	2.004 (1)	2.004 (1)	2.004(1)	Radical cluster	83(1)
III’	1.9880(5)	1.9860(5)	1.956(1)	Ti(III)	17(1)
ZnTi-2-A					
IV	2.004 (1)	2.004 (1)	2.004(1)	Radical cluster	99(1)
III’	1.9880(5)	1.9860(5)	1.956(1)	Ti(III)	1 (1)
P25-DA					
I	2.0025(5)	2.008(1)	2.034(2)	$HO_2^{\bullet}$	11(1)
VI	2.0042(5)	2.0022(5)	1.9975(5)	radical	61(1)
VII	2.0113(5)	2.0042(5)	2.0042(5)	radical	11(1)
VIII	1.992(2)	1.992(2)	1.962(2)	Ti(III)-anatase	1(1)
IX	1.973(2)	1.973(2)	1.950(5)	Ti(III)-rutile	15(1)

In a next experiment, the effect of the addition of an electron acceptor on the photocatalytic activity is tested. Electron acceptors may help to reduce the charge recombination after light-induced charge transfer and promote the mineralization of organic pollutants [4]. The earlier photocatalysis experiments (Figure 2) were repeated using H_2O_2 (1.8 mmol.L^{-1}) and $K_2S_2O_8$ (8 mmol.L^{-1}) as electron acceptors, respectively. The photocatalysis reaction was performed over ZnTi-2 at pH 5.2 and catalyst dosage of 1 g/L under visible light irradiation. The TOC of the solution was measured to determine the extent of mineralization. Table 3 lists the removal of SA

and TOC values after 6 h irradiation. As mentioned earlier, in the reaction system with LDH and SA alone, 40% SA can be removed and the TOC data indicate a 30% mineralization degree within 6 h of irradiation. The addition of H_2O_2 leads to a significant decrease in both the removal and mineralization degrees of SA. This may be attributed to the competitive adsorption of H_2O_2 and SA onto the surface of the LDH sheets, since H_2O_2 has a strong affinity to the surface Ti hydroxyls [45]. This seems to be confirmed by the decreased adsorption of the SA measured after the addition of H_2O_2 (Table 3), which may inhibit the CT and thus decrease the overall photocatalytic activity. In contrast, addition of the $K_2S_2O_8$ as electron acceptor remarkably improves the removal and mineralization degrees of SA (Table 3). Peroxydisulfate ions can accept electrons from the CB to produce sulfate ions and sulfate radicals, and then the latter can further accept electrons to produce sulfate ions, according to the following reactions [46].

$$S_2O_8^{2-} + e^-_{CB} \rightarrow SO_4^{2-} + SO_4^{-}\cdot, \quad SO_4^{-}\cdot + e^-_{CB} \rightarrow SO_4^{2-}$$

Besides the ability to accept photo-generated electrons, the beneficial effect of peroxydisulfate may be attributed to its relatively small competing adsorption onto the LDH surface (Table 3) due to its low affinity for the surface hydroxyl groups. In addition, the sulfate radicals can act as oxidizing agents and directly participate in the organic pollutant degradation processes [46].

Table 3. Effect of electron acceptor on the SA removal and mineralization (pH 5.2)

Electron acceptor	Removal of SA[a] (%)		TOC removal[d] (%)
	by initial adsorption[b]	by catalysis[c]	
without	7.6	32.7	29.8
H_2O_2	2.1	22.8	18.9
$K_2S_2O_8$	5.9	49.4	49.7

[a]measured at 296 nm using a UV-vis Spectrometer; [b]adsorption in dark, [c] 6h under visible light irradiation, [d]total organic carbon measured after visible light irradiation

In a final experiment (Figure S14), we test whether formation of •OH and/or O_2^- are implicated in the photocatalytic process. The addition of an excess of *tert*-butanol (TBA) as •OH scavenger to the photocatalytic mixture, hardly affected the photodegradation of SA, indicating that •OH radical formation does not play a role in the photocatalysis. On the other hand, when Ar was bubbled during the reaction, the degradation of SA was significantly suppressed, due to the lack of O_2 needed to generate O_2^-. Formation of O_2^- under visible light illumination of ZnTi-2 was indeed observed (Table 2, species I).

4. Discussion

Both the visually observed coloration and the UV-vis DR spectra (Figure 1B) confirm that contacting of SA to ZnTi LDH or to P25 leads to absorption of visible light. This is commonly attributed to the excitation of an electron from the HOMO of the organic molecule (here SA) to the CB of the semiconductor [2,4,10,13]. The fact that the XRD analysis revealed no change in the interlayer distance of the LDH contacted with SA indicates that SA is interacting with the surface of the LDH as opposed to replacing the intercalating carbonate anions. This is also confirmed by the presence of strong bands at circa 1500 and 1400 cm^{-1} in the DRIFT spectra of ZnTi-2 contacted with SA (Figure S4).

The photocatalytic tests (Figure 2A) show that this visible-light induced charge transfer (CT) initiates photodegradation. The best photodegradation of SA is obtained using the LDH with the

largest surface area and lowest Zn/Ti ratio (ZnTi-2). Interestingly, the SA removal increases linearly with the Ti/Zn ratio and extrapolates to zero activity for close to zero Ti content (Figure S15, supplementary material), which implies that the presence of Ti cations are crucial for the photocatalysis. The clear dependence of the photodegradation on the amount of LDH catalyst (Figure 2C) supports the hypothesis that the photodegradation is driven by a light-induced CT mechanism. A larger amount of catalyst allows more SA adsorption and thus more CT.

The optimal pH for the photodegradation of SA over ZnTi-2 is 5.2 (Figure 2B). The pH-dependence of the photocatalytic process can be explained by taking into account different factors. The SA molecules (or its anions) need to adsorb (bind) to the semiconductor surface to enable the visible-light driven HOMO→CB CT processes. pH values above the pK_a of SA (2.97) will favor the adsorption of the SA anions on positively charged surfaces. For ZnTi LDH with a point of zero charge (PZC) around 7, the surface will be positively charged at a pH value below 7. This explains why the optimal photocatalysis will occur between pH 3-7. Furthermore, corrosion of LDH may happen at lower pH values due to the dissolution of the metals in the brucite-like sheets [37]. This can explain the observation that the removal of SA at pH 4.1 and pH 5.2 is very similar at the beginning of the reaction but gradually differs with prolonged reaction time (Figure 2B).

The adsorption and binding of SA on the LDH and P25 surface is further confirmed by TGA/DTG experiments (Figure 3) showing extra weight loss at temperatures higher than the decomposition/combustion temperatures of the pristine semiconductors and SA materials, indicating the presence of Ti-bound SA molecules. Since the peaks appear at different temperatures in P25 contacted with SA than in the LDH contacted with SA, the binding strength

to the surface and the binding sites are (partially) different in the two materials. The TGA/DSC graphs also indicate a heterogeneity in the binding modes, which agrees with the model of heterogeneous interaction of SA with titania put forward by Regazzoni *et al*. [11].

The DRIFT spectra further confirm binding of SA and show the involvement of both the phenolic and carboxylic group in the metal binding (Figure 4). Some authors have used the stretching modes of the carboxyl group of the adsorbed SA to determine the specific binding of SA to surfaces of titania, but their interpretation of similar data is often conflicting [7-9, 11]. Because of the underlying contributions of the interlayer carbonates of the ZnTi LDH, a detailed analysis of these modes of the carboxyl group of the adsorbed SA is hampered. Plausible binding modes are those shown in Figure 5 and related complexes involving Zn(II), and they are probably co-existing in the LDH materials (see TGA/DSC results). This is also in line with the broad UV-vis DR absorption in the visible region (Figure 1B).

Several factors contribute to the observed differences in photocatalytic degradation of SA over the ZnTi LDH versus P25. Obviously, the material with the highest specific surface will allow for more adsorption of SA and thus more photodegradation, explaining in part the success of ZnTi-2. However, although ZnTi-4 and P25 have similar specific surfaces, the former is still degrading SA better. Since the photodegradation starts with a light-induced transfer of an electron from the HOMO of the adsorbed/bound SA molecule to the CB of the semiconductor, the relative position of the energy levels of SA versus the VB and CB will play a role. Given the different composition of LDH and P25, the absolute position of their CB and VB will differ, even though their bandgap is similar (3.1-3.3 eV, Figure 1 [34, 47]). The energy of the molecular orbitals of the bound SA molecules will be influenced by the type of binding to the surface.

A key limiting factor is the recombination of the charges after the CT process. Zhao *et al*. [47] derived that the electron–hole recombination process is significantly suppressed in ZnTi LDH as compared to bulk TiO_2, and attributed this to the higher density of surface defects as confirmed by their positron annihilation and extended X-ray absorption fine structure analyses. The highly dispersed TiO_6 octahedra and the intimate contact between Zn and Ti ions in the LDH matrix can increase the mobility of photo-generated electrons (metal to metal CT) and thus improve the efficiency of charge separation [20, 21, 47]. Our EPR studies show the formation of light-induced Ti(III) ions located on brookite-like positions (TiO_6) in ZnTi-2 with and without SA, highlighting the importance of the Ti atoms in the photocatalytic process in ZnTi LDH as follows also from the dependence of the photodegradation on the Ti/Zn ratio (Figure 2A, Figure S14). Density of states computations on ZnTi LDH materials showed that the Ti 3d-orbitals determine the CB minimum [34]. Ti ions on surface defect sites can have the 3d-orbital energies slightly below the CB and function as localized electron trap after photoexcitation of an electron.

Inspection of Figure 2A shows that the visible-light-induced removal of SA by P25 is finished after 2 hours, while this removal process is not yet finished after 6 hours on the LDH. This correlates with the TOC results that show that P25 is much less efficient in converting the adsorbed SA to CO_2. The EPR data show that the photodegradation of SA over P25 results in the formation of CO_2^-, a quite stable anion that may remain on the titania surface and thus block further adsorption and conversion of SA. In the LDH case, the degradation mechanism follows a route with different radical intermediates that eventually can be converted to CO_2 and hence free the surface to allow further adsorption and conversion of SA molecules. Since the absence of O_2 considerably reduces the photoactivity of the LDH materials, it seems likely that O_2^- formation is crucial in the degradation process. O_2^- can be formed by direct uptake of a CB electron by O_2 or

via the reaction of O_2 with Ti^{3+} to form Ti^{4+} - O_2^- with subsequent release of the superoxide radical. This seems to agree with the observed disappearance of the LI-EPR signals of the Ti^{3+} signals in ZnTi-2 when contacted longer with SA (Figure 6). Furthermore, LI EPR shows that pristine ZnTi-2 already absorbs some light at 447 nm with related formation of Ti(III) centers and O_2^- radicals (Table 2, Figure S8). Additional involvement of $^{\bullet}OH$ radicals can be ruled out on the basis of the photocatalytic experiments with the hydroxyl radical trap TBA.

Addition of electron acceptors are shown to influence the ZnTi-2 photoactivity. H_2O_2 reduces the photodegradation of SA, probably because H_2O_2 adsorbs equally well or better to the LDH surface than SA. In contrast, peroxydisulfate ions, adsorbing less effectively on the surface, increase the photoactivity, either due to an improved charge separation and/or further degradation of SA by the formed sulfate radicals.

5. Conclusion

ZnTi-containing layered double hydroxides were shown to be promising photocatalysts for the removal of salicylic acid under visible light irradiation in aqueous media. SA anions bind to the LDH surface and visible light can induce a charge transfer from the HOMO of SA to the conduction band of the semiconductor. This effect is also observed for P25 titania, but the photodegradation activity of ZnTi LDH is net superior to that of P25. The most active ZnTi LDH with Zn/Ti ratio of 2 can remove 40% of initial 50 mg/L SA in 6 h of visible light irradiation, compared to only 10% removal observed for P25. In the ZnTi LDH, the Ti ions play a crucial role in the photoactivity. The binding of SA to the semiconductor surface involves the phenolic and carboxylic groups of SA anions. Next to the type of binding and relative position of the CB versus the molecular orbitals of the adsorbed molecules, the high surface area of the ZnTi LDH

materials plays a beneficial role in the photocatalytic performance. Furthermore, the highly dispersed metal ions in MO_6 octahedra on LDH increase the charge-separation efficiency which is the main limiting factor in this type of photodegradation processes. Our results also show clear differences in the type of radical intermediates that are formed when comparing SA photodegradation on ZnTi LDH and on P25. CO_2^- is formed in the P25 case, while its formation is not observed for ZnTi LDH. Superoxide radicals (and O_2) play a crucial role in the photocatalytic behavior, while hydroxyl radicals are not implicated in the photodegradation of SA. Addition of the electron acceptor peroxydisulfate can significantly improve both the degradation and mineralization degrees of SA, while H_2O_2 hampers this process.

Based on the present investigation, ZnTi LDH emerge as more effective substrates than pure TiO_2 for the visible-light induced photodegradation of colorless organic pollutants under visible light irradiation.

Acknowledgements

H. Wang greatly acknowledges for the financial support from the National Natural Science Foundation of China (No. 21506176) and China Scholarship Council. E. M. Seftel greatly acknowledges the Fund for Scientific Research-Flanders (FWO- Vlaanderen) for financial support. R.-G. Ciocarlan acknowledges the FWO-Flanders (project nr. G038215N) for financial support. S. Van Doorslaer, P. Cool and B. Cuypers thank the University of Antwerp for GOA-BOF funding (28312).

References

1. M. Pelaez, N. T. Nolan, S. C. Pillai, M. K. Seery, P. Falaras, A. G. Kontos, P. S. M. Dunlop, J. W. J. Hamilton, J. A. Byrne, K. O'Shea, M. H. Entezari, D. D. Dionysiou, A review on the visible light active titanium dioxide photocatalysts for environmental applications, Appl. Catal. B-Environ.,125 (2012) 331-349.
2. H. Park, H. Kom, G. Moon, W. Choi, Photoinduced charge transfer processes in solar photocatalysis based on modified TiO_2, Energy Environ. Sci, 9 (2016) 411-433.
3. G. Zhang, G. Kim, and W. Choi, Visible light driven photocatalysis mediated via ligand-to-metal charge transfer (LMCT): an alternative approach to solar activation of titania, Energy Environ. Sci, 7 (2014) 954-966.
4. N. Wang, L. Zhu, Y. Huang, Y. She, Y. Yu, H. Tang, Drastically enhanced visible-light photocatalytic degradation of colorless aromatic pollutants over TiO_2 via a charge-transfer-complex path: A correlation between chemical structure and degradation rate of the pollutants, J. Catal., 266 (2009) 199-206.
5. N. Ratola, A. Cincinelli, A. Alves, A.Katsoyiannis, Occurrence of organic microcontaminants in the wastewater treatment process. A mini review, J. Hazard. Mater., 239-240 (2012) 1-18.
6. C. Miege, J. M. Choubert, L. Ribeiro, M. Eusèbe, M. Coquery, Fate of pharmaceuticals and personal care products in wastewater treatment plants-Conception of a database and first results. Environ. Pollut., 157 (2009) 1721-1726.
7. T. D. Savić, M. I. Čomor, N. D. Abazović, Z. V. Šaponjić, M. T. Marinović-Cincović, D. Ž. Vejković, S. D. Zarić, I. A. Janković, Anatase nanoparticles surface modified with fused ring salicylate-type ligands (1-hydroxy-2-naphthoic acids): A combined DFT and experimental study. J. Alloys Compd., 630 (2015)226-235,

8. T. D. Savić, Z. V. Šaponjić, M. I. Čomor, J. M. Nedeljković, M. D. Dramićanin, M. G. Nikolić, D. Ž. Vejković, S. D. Zarić, I. A. Janković, Surface modification of anatase nanoparticles with fused ring salicylate-type ligands (3-hydroxy-2-naphthoic acids): a combined DFT and experimental study of optical properties. Nanoscale, 5 (2013) 7601-7612.
9. A. D. Weisz, L García Rodenas, P. J. Morando, A. E. Regazzoni, M. A. Blesa, FTIR study of the adsorption of single pollutants and mixtures of pollutants onto titanium dioxide in water: oxalic and salicylic acids. Catal. Today, 76 (2002) 103-112,
10. S. Varaganti, G. Ramakrishna, Dynamics of Interfacial Charge Transfer Emission in Small Molecule Sensitized TiO_2 Nanoparticles: Is It Localized or Delocalized? J. Phys. Chem. C, 114 (2010) 13917-13925.
11. A. E. Regazzoni, P. Mandelbaum, M. Matsuyoshi, S. Schiller, S. A. Bilmes, M. A. Blesa, Adsorption and Photooxidation of Salicylic Acid on Titanium Dioxide: A Surface Complexation Description. Langmuir, 14 (1998) 868-874.
12. L. Shun-Xing, Z. Feng-Ying, C. Wen-Lian, H. Ai-Qin, X. Yu-Kun, Surface modification of nanometer size TiO_2 with salicylic acid for photocatalytic degradation of 4-nitrophenol. J. Hazard. Mater. B, 135 (2006) 431-436.
13. M. F. Nsib, A. Maayoufi, N. Moussa, N. Tarhouni, A. Massouri, A, Houas, Y. Chevalier, TiO_2 modified by salicylic acid as a photocatalyst for the degradation of monochlorobenzene via Pickering emulsion way. J. Photochem. Photobiol. A: Chemistry, 251 (2013) 10-17.

14. O. V. Makarova, T. Rajh, M. C. Thurnauer, A. Martin, P. A. Kemme, D. Cropek, Surface Modification of TiO_2 Nanoparticles For Photochemical Reduction of Nitrobenzene. Environ. Sci. Technol., 34 (2000) 4797-4803.
15. D. G. Evans, R. C. T. Slade, Structural aspects of layered double hydroxides, Struct. Bond. 119 (2006) 1-87.
16. C. G. Silva, Y. Bouizi, V. Fornés, H. García, Layered Double Hydroxides as Highly Efficient Photocatalysts for Visible Light Oxygen Generation from Water. J. Am. Chem. Soc., 131 (2009) 13833-13839.
17. L. Mohapatra, K. Parida, A review on the recent progress, challenges and perspective of layered double hydroxides as promising photocatalysts, J. Mater. Chem A, 4 (2016) 10744-10766
18. Y. Lee, J. H. Choi, H. J. Jeon, J. W. Lee, J. K. Kang, Titanium-embedded layered double hydroxides as highly efficient water oxidation photocatalysts under visible light. Energy Environ. Sci., 4 (2011) 914-920.
19. E. M. Seftel, M. C. Puscasu, M. Mertens, P. Cool, G. Carja, Fabrication of CeO_2/LDH self-assemblies with enhanced photocatalytic performance: A case study on ZnSn-LDH matrix. Appl. Catal. B, 164 (2015) 251-260.
20. E. M. Seftel, M. C. Puscasu, M. Mertens, P. Cool, G. Carja, Assemblies of nanoparticles of CeO_2-ZnTi-LDH and their derived mixed oxides as novel photocatalytic systems for phenol degradation. Appl. Catal. B, 150-151 (2014) 157-166.
21. E. M. Seftel, E. Popovici, M. Mertens, E. A. Stefaniak, R. Van Grieken, P. Cool, E. F. Vansant, Sn^{IV}-containing layered double hydroxides as precursors for nano-sized ZnO/SnO_2 photocatalysts. Appl. Catal. B, 84 (2008) 699-705.

22. G. Carja, E. F Grosu, M. Mureseanu, D. Lutic, A family of solar light responsive photocatalysts obtained using Zn^{2+} Me^{3+} (Me = Al/Ga) LDH doped with Ga_2O_3 and In_2O_3 and their derived mixed oxides: a case study of phenol/4-nitrophenol decomposition. Catal. Sci, 7(22), 5402-5412.

23. G. Mikami, F. Grosu, S. Kawamura, Y. Yoshida, G. Carja, Y. Izumi, Harnessing self-supported Au nanoparticles on layered double hydroxides comprising Zn and Al for enhanced phenol decomposition under solar light. Appl. Catal. B, 199, 260-271.

24. M. Darie, E. M. Seftel, M. Mertens, R. G. Ciocarlan, P. Cool, G. Carja, Harvesting solar light on a tandem of Pt or Pt-Ag nanoparticles on layered double hydroxides photocatalysts for p-nitrophenol degradation in water. Appl. Clay Sci., 182, 105250.

25. L. Sobhana, M. Sarakha, V. Prevot, P. Fardim, Layered double hydroxides decorated with Au-Pd nanoparticles to photodegradate Orange II from water. Appl. Clay Sci., 134, 120-127.

26. M. Shao, J. Han, M. Wei, D. G. Evans, X. Duan, The synthesis of hierarchical Zn-Ti layered double hydroxide for efficient visible-light photocatalysis. Chem. Eng. J., 168 (2011) 519-524.

27. O. Saber, H. Tagaya, New Layered Double Hydroxide, Zn-Ti LDH : Preparation and Intercalation Reactions. J. Inclusion Phenom. Macrocyclic Chem., 45 (2003) 109-116.

28. S. Stoll, A. Schweiger, EasySpin, a comprehensive software package for spectral simulation and analysis in EPR. J. Magn. Reson., 178 (2006) 42-55.

29. W. H. Zhang, X. D. Guo, Z. Y. Qian, Preparation of Ni(II)/Ti(IV) layered double hydroxide at high supersaturation. J. Eur. Ceram. Soc, 28 (2008) 1623-1629.

30. E. M. Seftel, E. Popovici, M. Mertens, G. Van Tendeloo, P. Cool, E. F. Vansant, The influence of the cationic ratio on the incorporation of Ti^{4+} in the brucite-like sheets of layered double hydroxides. Micropor. Mesopor. Mater., 111 (2008) 12-17.
31. M. Silion, D. Hritcu, M. I. Popa, Intercalation of salicylic acid into ZnAl layered double hydroxides by ion-exchange and coprecipitation method, J. Optoelectron. Adv. M., 11 (2009) 528-534.
32. S. Xu, J. Yu, W. Wu, L. Xue, Y. Sun, Synthesis and characterization of layered double hydroxides intercalated by UV absorbents and their application in improving UV aging resistance of bitumen, Appl. Clay Sci., 114 (2015) 112-119.
33. M. Ramli, M. Z. Mohd, K. Yusoff, Preparation and characterization of an anti-inflammatory agent based on a zinc-layered hydroxide-salicylate nanohybrid and its effect on viability of Vero-3-cells, Int. J. Nanomed. 8 (2013) 297-306.
34. X.-R. Wang, Y. Li, L.-P. Tang, W. Gan, W. Zhou, Y.-F. Zhao, D.-S. Bai, Fabrication of Zn-Ti layered double hydroxide by varying cationic ratio of Ti^{4+} and its application as UV absorbent, Chin. Chem. Lett., 28 (2017) 394-399.
35. S. Tunesi, M. A. Anderson, Surface Effects in Photochemistry: An in Situ Cylindrical Internal Reflection-Fourier Transform Infrared Investigation of the Effect of Ring Substituents on Chemisorption onto TiO_2 Ceramic Membranes, Langmuir, 8 (1992) 487-495.
36. F. Cavani, F. Trifiro, A. Vaccari, Hydrotalcite-type anionic clays: Preparation, properties and applications. Catal. Today, 11 (1991) 173-301.

37. X. Shu, J. He, D. Cheng, Y. Wang, Tailoring of Phase Composition and Photoresponsive Properties of Ti-Containing Nanocomposites from Layered Precursor. J. Phys. Chem. C, 112 (2008) 4151-4158.

38. S. G. Kumar, L.G. Devi, Review on Modified TiO_2 Photocatalysis under UV/Visible Light: Selected Results and Related Mechanisms on Interfacial Charge Carrier Transfer Dynamics. J. Phys. Chem. A, 115 (2011) 13211-13241.

39. M. Fittipaldi, D. Gatteschi, P. Fornasiero, The power of EPR techniques in revealing active sites in heterogeneous photocatalysis: The case of anion doped TiO_2. Catal. Today, 206 (2013) 2-11.

40. E. Morra, E. Giamello, M. Chiesa, J. Magn. Reson. 280 (2017) 89-102.

41. A. L. Attwood, D. M. Murphy, J. L Edwards, T. A. Egerton, R. W. Harrison, An EPR study of thermally and photochemically generated oxygen radicals on hydrated and dehydrated titania surfaces. Research on Chemical Intermediates, 29 (2003) 449-465.

42. D. C. Hurum, A. G. Agrios, K. A. Gray, T. Rajh, M. C. Thurnauer, Explaining the Enhanced Photocatalytic Activity of Degussa P25 Mixed-Phase TiO_2 Using EPR. J. Phys. Chem. B 107 (2003) 4545-4549

43. M. Chiesa, E. Giamello, M. Che, EPR Characterization and Reactivity of Surface-Localized Inorganic Radicals and Radical Ions. Chemical Reviews, 110 (2010) 1320-1347.

44. E. Carter, A.F. Carley, and D.M. Murphy, Free-Radical Pathways in the Decomposition of Ketones over Polycrystalline TiO2: The Role of Organoperoxy Radicals. ChemPhysChem, 8 (2007) 113-123.

45. X. Li, C. Chen, J. Zhao, Mechanism of Photodecomposition of H_2O_2 on TiO_2 Surfaces under Visible Light Irradiation. Langmuir, 17 (2001) 4118-4122.
46. S. Malato, J. Blanco, C. Richter, B. Braun, M. I. Maldonado, Enhancement of the rate of solar photocatalytic mineralization of organic pollutants by inorganic oxidizing species. Appl. Catal. B, 17 (1998) 347-356.
47. Y. Zhao, P. Chen, B. Zhang, D. S. Su, S. Zhang, L. Tian, J. Lu, Z. Li, Z. Cao, B. Wang, M. Wei, D. G. Evans, X. Duan, Highly Dispersed TiO_6 Units in a Layered Double Hydroxide for Water Splitting, Chem. Eur. J., 18 (2012) 11949-11958.

Supplementary material for

ZnTi layered double hydroxides as photocatalysts for salicylic acid degradation under visible light irradiation

Hao Wang[a,b,], Elena M. Seftel[b,c], Radu G. Ciocarlan[b], Bert Cuypers[d], Myrjam Mertens[c], Sabine Van Doorslaer[d], Yan Wu[a], Pegie Cool[b,*]

S1. XRD and DRIFT characterization of ZnTi LDHs

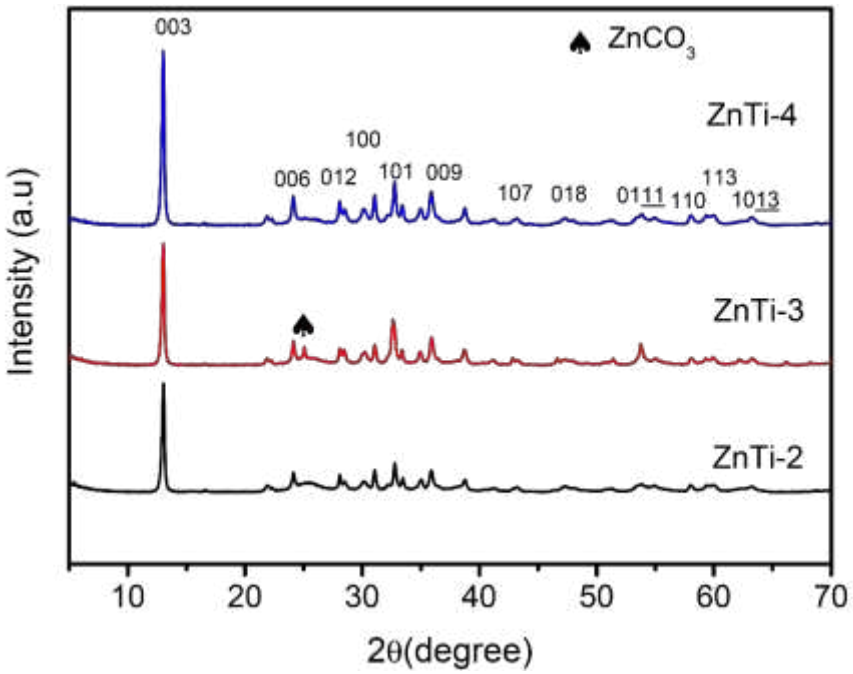

Figure S1. XRD analysis of the ZnTi LDHs under study.

Their XRD patterns are shown in Figure S1. For all the samples, a strong refection around 13.1° assigned to the (003) crystal plane and a series of reflections assigned to (006), (009), (100), (101), (012), (110) and (113) crystal planes are observed, which can be indexed to typical LDH-layered materials. The positions of the reflections are in agreement with those reported in literature [1,2]. It is noted that the d-spacing of (003) crystal plane is around 0.67 nm, which is

smaller than normal LDHs containing M^{3+} (around 0.77 nm). This may be attributed to the strong electrostatic interaction between the Ti^{4+}-containing brucite-like sheets and the interlayer carbonate anions [1]. The (003) reflection is sharp and narrow, indicating a well-ordered lamellar structure. Some weak reflections at 25.1, 30.2 and 35.8° were also observed, which are assigned to the small amounts of $ZnCO_3$ impurities [1].

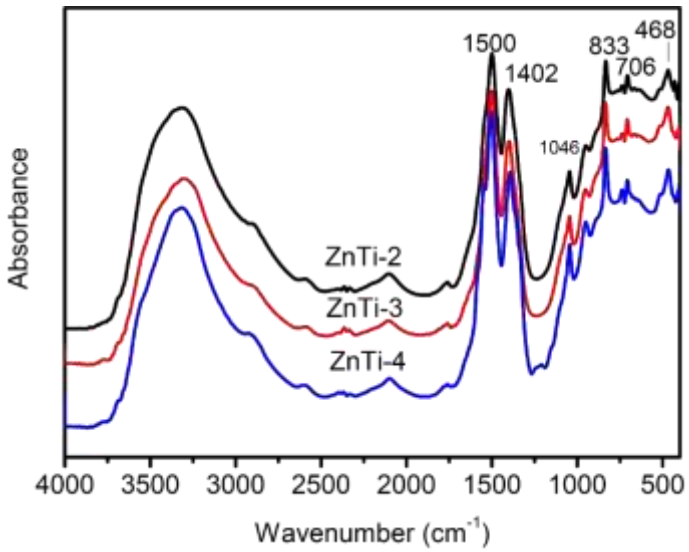

Figure S2. DRIFT spectra of the ZnTi LDHs under study.

The DRIFT spectra of the three ZnTi LDH samples are depicted in Figure S2. All the samples show similar absorption bands. The bands in the range of 400–900 cm^{-1} may be attributed to the M-O and M-OH lattice vibration modes in the brucite-like sheets [3]. The band of the carbonate anions in the interlayer is normally observed at 1376 cm^{-1} in the LDHs consisting of M^{3+}. It is, however, shifted and split into two distinctive bands at circa 1500 and 1400 cm^{-1}, which may be attributed to the restricted symmetry in the interlayer space due to the presence of tetravalent Ti^{4+} cations in the layered structure [2,4]. The Ti^{4+} cations incorporated in the layer lead to an excess of positive charges. As such, the electrostatic attraction between the brucite layers and the interlayer carbonate anions is stronger as compared with the M^{3+}-containing LDHs, which results in a decrease of the symmetry of the carbonate anions from D_{3h} for the free anions to C_{2v} due to the disordered nature of the interlayer space [2-4]. In addition, the weak band at 1046 cm^{-1} can be ascribed to the ν_1 mode of carbonate in the interlayer [2,5]. These results correlate well with

the XRD observations indicating a decrease in the interlayer distance due to the higher positive charged brucite-like sheets.

S2. TGA/DTG profiles of pristine ZnTi LDH materials

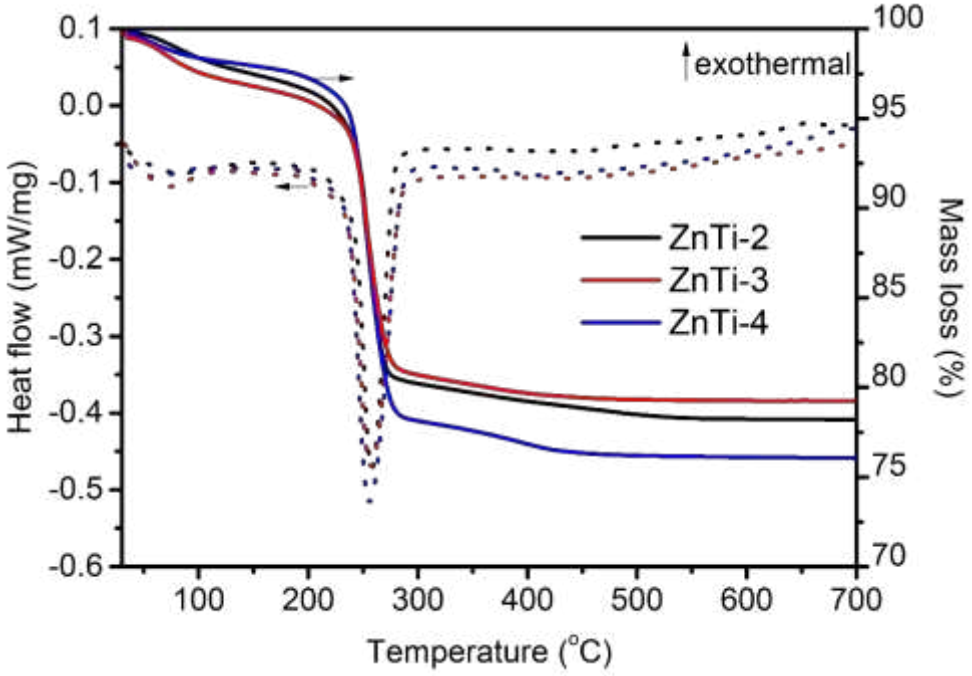

Figure S3. TGA/DTG profiles of the pristine ZnTi LDHs under study.

S3. DRIFT analysis of ZnTi-2 and P25 after contacting with SA

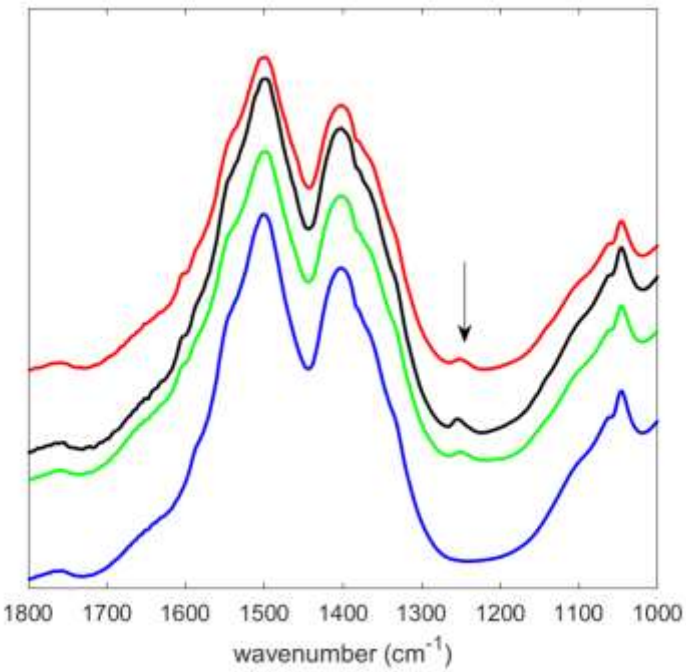

Figure S4. (from top to bottom) DRIFT spectra of ZnTi-2-DA (red), ZnTi-2-D (black), ZnTi-2-A (red), pristine ZnTi-2 (blue). All spectra are dominated in this region by the bands of the carbonate anions. Small extra features are observed in the samples contacted with SA in dark or visible light (the arrow indicates such an extra feature). In Figure 4 (main text) these features are highlighted in the spectrum obtained after subtraction of the DRIFT spectrum of ZnTi-2 from that of ZnTi-2-DA.

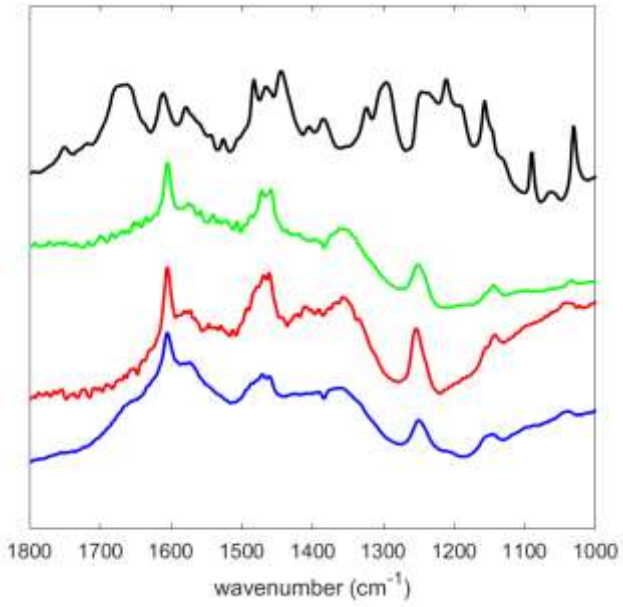

Figure S5. From top to bottom: (black) DRIFT spectrum of salicylic acid. Difference spectrum obtained by subtracting the DRIFT spectrum of ZnTi-2 from that of (green) ZnTi-2-DA, (red) ZnTi-2-D, (blue) ZnTi-2-A.

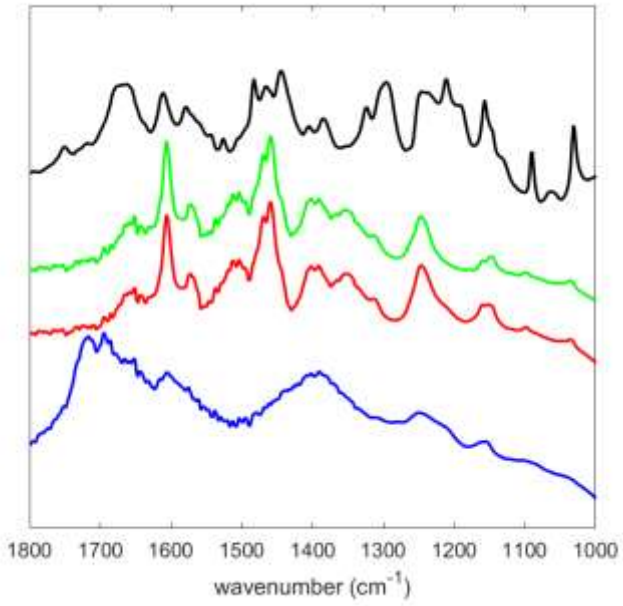

Figure S6. From top to bottom: (black) DRIFT spectrum of salicylic acid. Difference spectrum obtained by subtracting the DRIFT spectrum of P25 from that of (green) P25-DA, (red) P25-D, (blue) P25-A.

S4. Light-induced EPR analysis

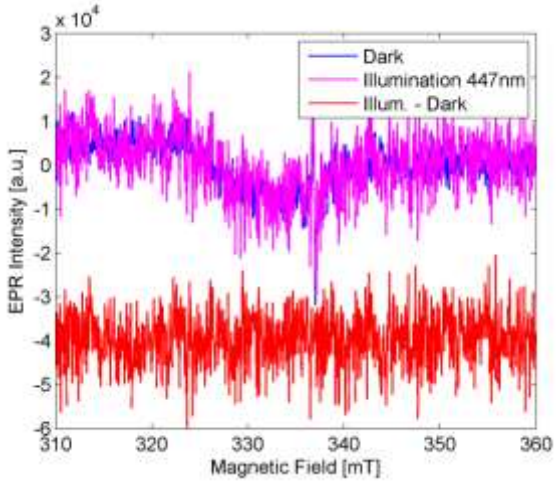

Figure S7. X-band CW EPR spectrum before (blue) and after (magenta) *in situ* illumination (447 nm) of salicylic acid (SA) at low temperature (10 K). Red: difference spectrum.

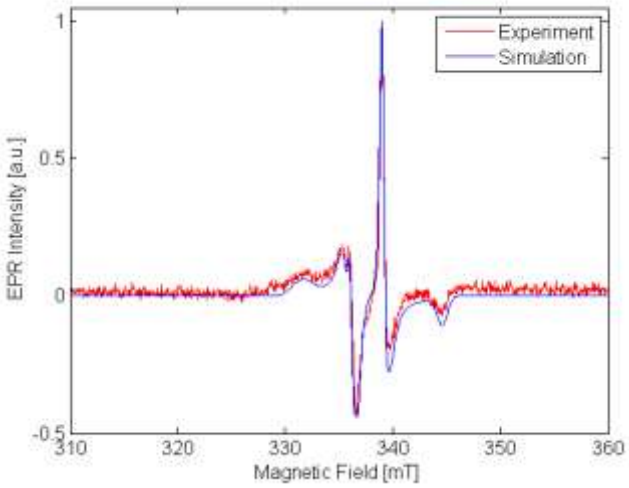

Figure S8. X-band LI-EPR spectrum (difference between spectrum recorded after and before 30 min. illumination with 447 nm laser light, 10 K) of pristine ZnTi-2. Experiment (red), simulation assuming the contributions indicated in Table 2 of the main text (blue). Spectra are represented normalized to the highest intensity for comparison.

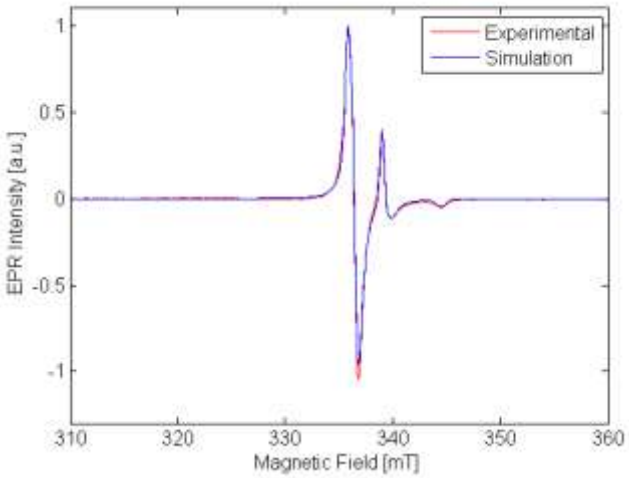

Figure S9. X-band LI-EPR spectrum (difference between spectrum recorded after and before 30 min. illumination with 447 nm laser light, 10 K) of ZnTi-2-D. Experiment (red), simulation assuming the contributions indicated in Table 2 of the main text (blue). Spectra are represented normalized to the highest intensity for comparison.

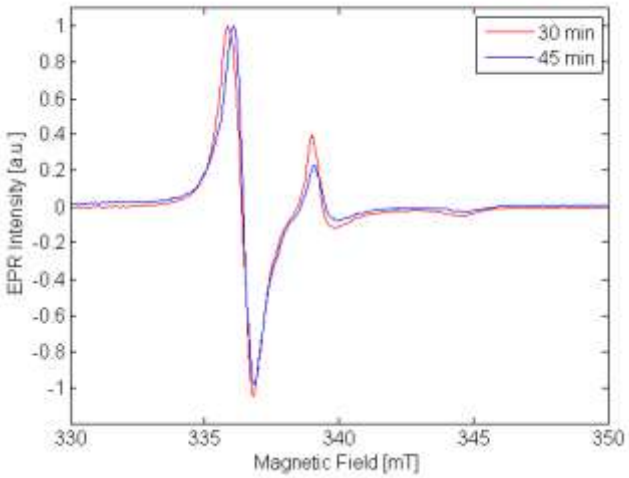

Figure S10. Comparison of X-band LI-EPR spectrum (difference between spectrum recorded after and before illumination with 447 nm laser light, 10 K) of ZnTi-2-D for different times of illumination. The spectra are normalized to the highest intensity to allow comparison of the spectral shape. We see a narrowing of the contribution of the low-field signal due to the disappearance of the contribution of center V.

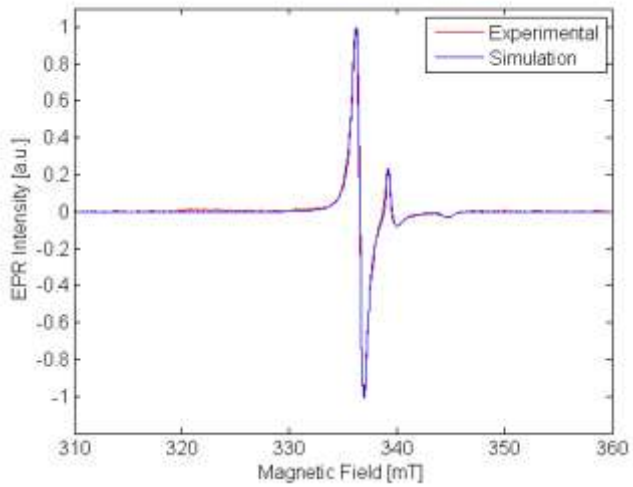

Figure S11. X-band LI-EPR difference spectrum (difference between spectrum recorded after and before 30 min. illumination with 447 nm laser light, 10 K) of ZnTi-2-DA. Experiment (red), simulation assuming the contributions indicated in Table 2 of the main text (blue). Spectra are represented normalized to the highest intensity for comparison.

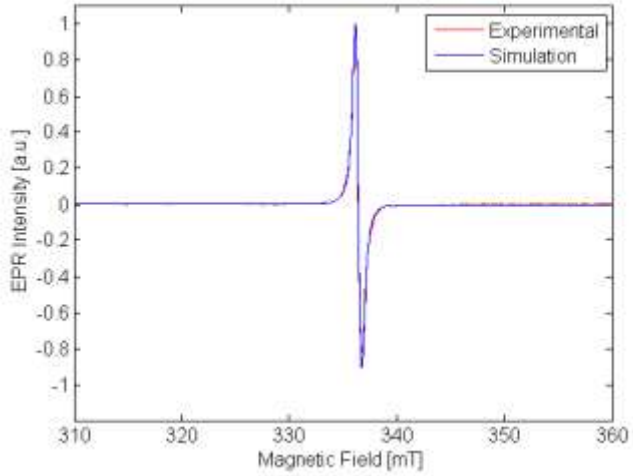

Figure S12. X-band LI-EPR difference spectrum (difference between spectrum recorded after and before 30 min. illumination with 447 nm laser light, 10 K) of ZnTi-2-A. Experiment (red), simulation assuming the contributions indicated in Table 2 of the main text (blue). Spectra are represented normalized to the highest intensity for comparison.

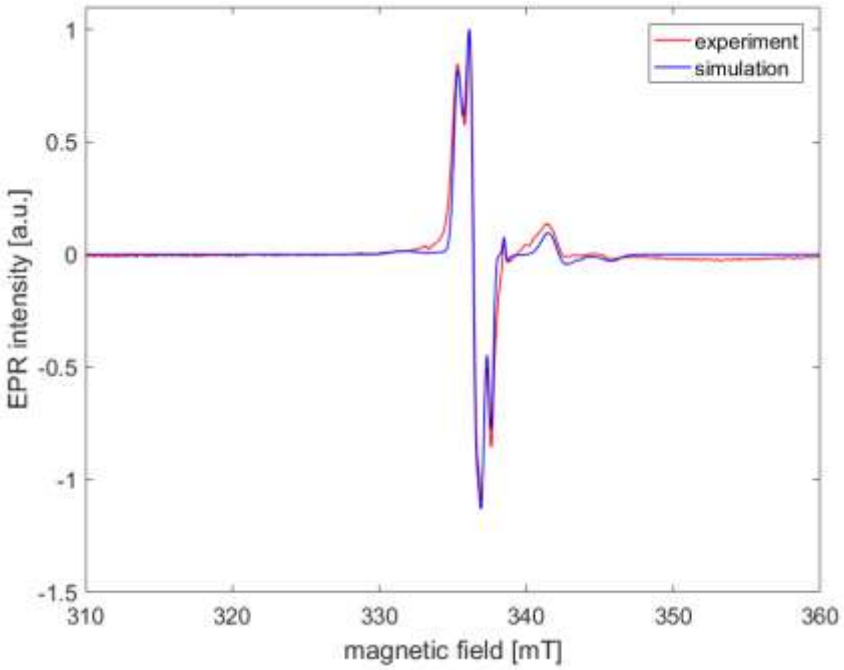

Figure S13. X-band LI-EPR difference spectrum (difference between spectrum recorded after and before 45 min. illumination with 447-nm laser light, 10 K) of P25-DA. Experiment (red), simulation assuming the contributions indicated in Table 2 of the main text (blue). Spectra are represented normalized to the highest intensity for comparison

S5. Data of photocatalytic degradation

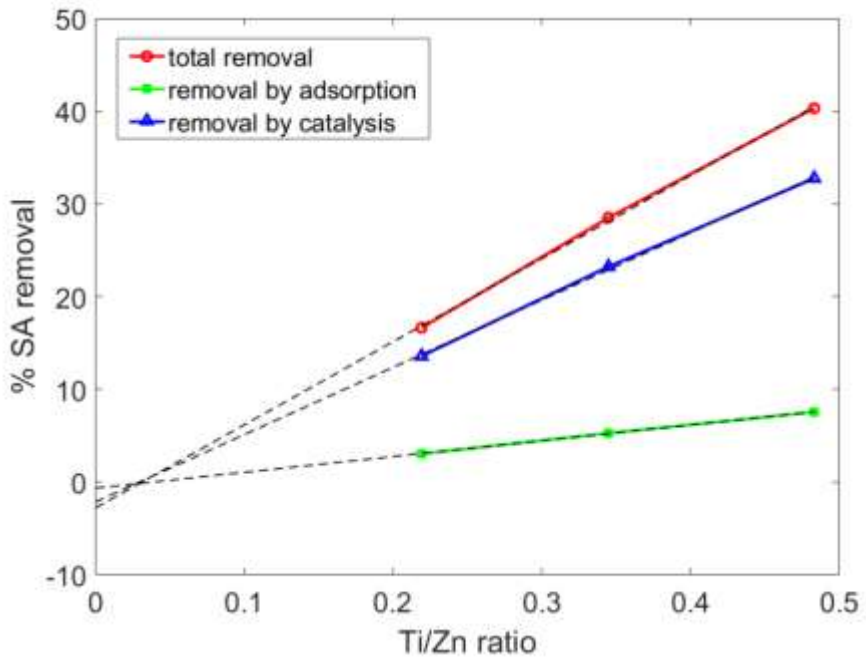

Figure S14. Removal of SA by ZnTi LDHs versus Ti/Zn ratio. The data points correspond to the points after 6h photocatalysis (Figure 2A, main text). Linear extrapolation gives zero SA removal for Ti/Zn ratio near 0. This suggests that the Ti/Zn ratio plays a dominant role in the photoactivity.

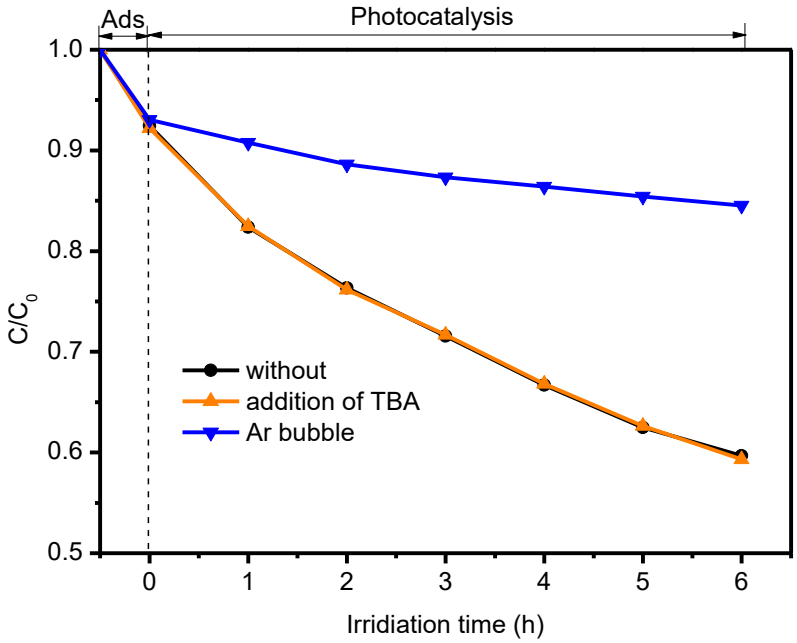

Figure S15. Photodegradation of SA by ZnTi-2 with TBA or under Ar bubble. The addition of 5 mmol TBA has no influence on the activity of ZnTi-2. However, Ar bubble leads to a significant decrease in the activity.

References

1. M. Shao, J. Han, M. Wei, D. G. Evans, X. Duan, The synthesis of hierarchical Zn-Ti layered double hydroxide for efficient visible-light photocatalysis. Chem. Eng. J., 168 (2011) 519-524.
2. O. Saber, H. Tagaya, New Layered Double Hydroxide, Zn-Ti LDH : Preparation and Intercalation Reactions. J. Inclusion Phenom. Macrocyclic Chem., 45 (2003) 109-116.
3. Y. Lee, J. H. Choi, H. J. Jeon, J. W. Lee, J. K. Kang, Titanium-embedded layered double hydroxides as highly efficient water oxidation photocatalysts under visible light. Energy Environ. Sci., 4 (2011) 914-920.

4. W. H. Zhang, X. D. Guo, Z. Y. Qian, Preparation of Ni(II)/Ti(IV) layered double hydroxide at high supersaturation. J. Eur. Ceram. Soc, 28 (2008) 1623-1629.
5. E. M. Seftel, E. Popovici, M. Mertens, G. Van Tendeloo, P. Cool, E. F. Vansant, The influence of the cationic ratio on the incorporation of Ti^{4+} in the brucite-like sheets of layered double hydroxides. Micropor. Mesopor. Mater., 111 (2008) 12-17.